International Journal of Environmental Science and Technology
https://doi.org/10.1007/s13762-025-06751-4

ORIGINAL PAPER

Multi-mechanistic modeling and experimental validation for pharmaceutical removal through novel clew-shaped ZnO: diclofenac removal from aqueous environment

N. Allahgholi[1] · S. M. Miraboutalebi[2] · M. Sohrabi[3] · T. V. Nguyen[2] · S. Vigneswaran[2] · G. McKay[4]

Received: 21 April 2025 / Revised: 30 July 2025 / Accepted: 28 August 2025

Abstract
A modified ZnO adsorbent, named clew-shaped ZnO (CSZN), was introduced as a highly effective material for removing diclofenac (DCF). Compared to smooth ZnO (SZN), CSZN showed a more than 250% increase in adsorption capacity under the same experimental conditions. This improvement was assigned to more active adsorption sites and a larger effective surface area. The study investigated various operating parameters and their effects on DCF adsorption onto SZN and CSZN. To optimize the adsorption model, both kinetic and isotherm models were evaluated. Two multi-mechanism isotherm models were employed to improve the predictive accuracy of the adsorption process. The nonlinear multi-mechanism model showed that the Lan-Lan model provided the best predictive capability, having a significantly lower Sum of Squares Error (SSE) of 1735, compared to 5505 for a single isotherm model. This finding emphasized the better accuracy of the multi-mechanistic approach, particularly the Lan-Lan model, in predicting DCF adsorption behavior onto CSZN. Overall, the study confirms that CSZN can be considered as a highly efficient adsorbent for DCF removal from wastewater as well as the power of the multi-mechanistic approach for offering better models.

Editorial responsibility: Samareh Mirkia.

✉ T. V. Nguyen
Tien.Nguyen@uts.edu.au

[1] Department of Civil, Chemical, Environmental, and Materials Engineering-DICAM, Alma Mater Studiorum, Universita di Bologna, Bologna, Italy

[2] School of Civil and Environmental Engineering, Faculty of Engineering and IT, University of Technology Sydney, 15 Broadway, Ultimo, NSW 2007, Australia

[3] Department of Applied Chemistry, Faculty of Science, Islamic Azad University, South Tehran Branch, Iran

[4] Division of Sustainability, College of Science and Engineering, Hamad Bin Khalifa University, Education City, Qatar Foundation, Doha, Qatar

Published online: 14 September 2025

Graphical abstract

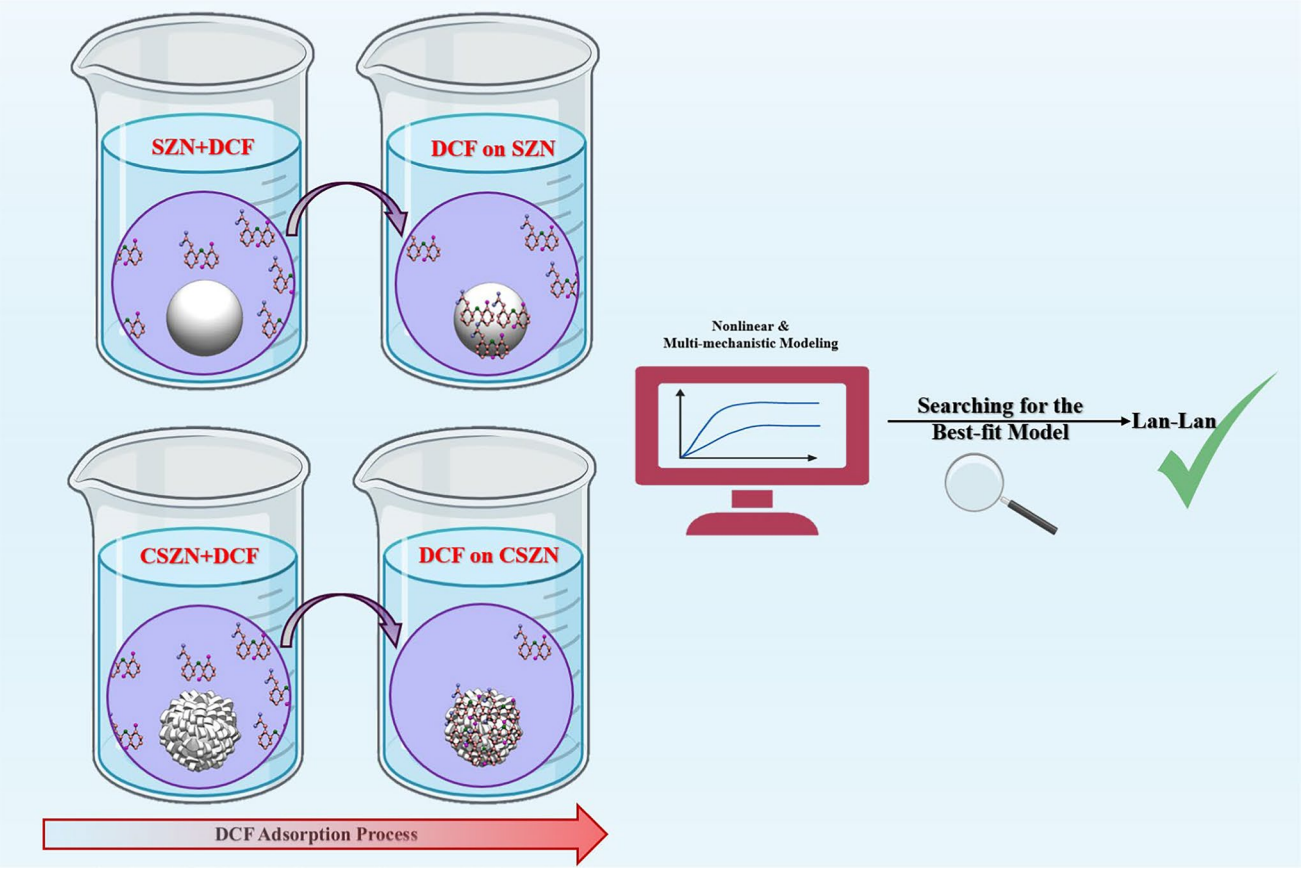

Keywords Surface modification · Pharmaceutical wastewater · High-capacity adsorbent · Multi-mechanistic modeling

Introduction

The sharp increase in the world's population has strengthened concerns regarding millions of people's access to clean and safe drinking water. Additionally, the expansion of industrial activities continues to trigger mass discharges of different kinds of dangerous pollutants to sewage systems or even into the natural environment without sufficient treatment of any kind. This subsequently leads to serious contamination of underground water resources (Alyasi et al. 2021; Obar et al. 2024; Yan et al. 2022). Pharmaceutical pollutants are addressed as newly established ones compared to others found in aquatic environments, which is due to the lack of an appropriate removal technique in wastewater or water treatment systems (Araujo et al. 2021; de Souza dos Santos et al. 2020).

Diclofenac (DCF) is a substance with low biodegradability characteristics, and it is a nonsteroidal anti-inflammatory drug that is mainly prescribed to treat pain (Poddar et al. 2024). DCF can threaten some aquatic creatures, including fish, crustaceans and amphibians. Some serious outcomes like slowed growth, decreased reproductive rates, and developmental abnormalities can be addressed as a result of exposure to DCF. It is important to note that there is also a major concern about DCF; it may interact with other water pollutants from miscellaneous sources, potentially leading to major environmental harm (Kandaswamy et al. 2024; Wolska et al. 2025). It has been detected in soil and drinking water due to its wide consumption and lack of efficient treatment techniques. Even in a trace amount in wastewater systems, its continuous discharge from hospital sewage systems or wastewater treatment plants is becoming a serious matter that needs special attention given the long-term impact. In March 2015, DCF was listed on the watch list of the Commission Implementing Decision of the EU as a pharmaceutical waste. Subsequently, its hazardous characteristics for the environment and human body health must be taken into consideration (Dzimitrowicz et al. 2024; Shamsudin et al. 2022). The main DCF characteristics are presented in Table S1, in Supplementary Information (SI).

DCF has shown to be highly persistent against conventional treatment methods like filtration, coagulation, and sedimentation, and it has been found in concentrations higher than the Predicted No Effect Concentration (PNEC) in treated wastewater, proving that conventional wastewater treatment methods may not effectively remove this compound (Alessandretti et al. 2021; Devaisy et al. 2022). Consequently, degrading DCF, which is one of the pharmaceutical pollutants using environmentally friendly materials, is not an easy process. For example, the DCF concentration only decreased from 0.25 to 0.215 ppb in a wastewater treatment unit employing conventional treatment methods (de Souza dos Santos et al. 2020; Shamsudin et al. 2022). Many methods, such as biological treatment (Chyoshi et al. 2022; Elshikh et al. 2022), photocatalytic membrane (Dekkouche et al. 2022), adsorptive membrane (Carmo et al. 2022) and adsorption (Moradi et al. 2022), were established to remove DCF from wastewater. Despite all the recent advances that have been made in wastewater treatment for removing DCF, there is an urgent need to find new promising techniques and materials that are more feasible and efficient.

Nanoparticles play a critical role in technologies related to environmental protection and sustainability (Areeb et al. 2021). Metal and metal oxide nanoparticles or nanotubes like Ni, Zn, Fe, ZnO, TiO_2 and γ-Al_2O_3 exhibit a favorable ability to adsorb contaminants, especially pharmaceutical compounds from aqueous solutions thanks to having high activity and large surface areas. They naturally have adequate capacity and desirable selectivity that make them proficient in the extensive removal of pharmaceutical contaminants (Almasri et al. 2019; Dekkouche et al. 2022; Negarestani et al. 2022; Nodehi et al. 2022; Rajiv et al. 2021; Shayesteh et al. 2022).

Numerous nanomaterials are applied to wastewater/water treatment, but most of them do not have a high surface area or only an adsorption capacity, and furthermore, the production costs are high (Alharthi et al. 2020). Hence, finding a way to improve adsorbent surface area and activity in the purification processes is highly important. One of the ways is to change the surface morphology, which has been recently addressed as a workable way to increase nanoparticle adsorption activity in wastewater treatment or water purification processes. In this way, the higher active surface area is accessible and will offer a reasonable adsorption capacity (Ahsani-Namin et al. 2022; Al-Musawi et al. 2022; Pathy et al. 2022). One practical example is employing hedgehog-like micro/nanostructure nickel in the separation process of oil and water mixture (Shayesteh et al. 2022). Although DCF removal has been investigated regarding improved DCF adsorption, advances in adsorption technology still suffer from time-consuming processes and the inability to remove large amounts. Consequently, there exist opportunities for new and surface-modified nanostructure adsorbents.

This research paper identified smooth ZnO (SZN) as having a reasonable capacity to adsorb DCF from wastewater. Thus, the new clew-shaped ZnO (CSZN) was synthesized, and its adsorption kinetics behavior and efficiency for DCF adsorption from wastewater were compared with that of SZN. To better understand the adsorption events, a multi-mechanistic isotherm modeling approach was developed for DCF removal from an aqueous system using CSZN adsorbent. In this approach, two isotherm equations were employed to model the experimental data. The basis of the new approach is to divide the experimental data into two main regions and model them with two isotherm equations to generate better accuracy and prediction.

Materials and methods

Chemicals

Sodium hydroxide anhydrous (≥ 98%, pellets), zinc nitrate hexahydrate (≥ 98%), sodium citrate dihydrate, and hexamethylenetetramine (≥ 99.0%) were purchased from Sigma Aldrich. All the mentioned chemicals were used without any further purification.

Preparations of SZN and CSZN

SZN was initially prepared[1] to utilize the following procedure: 7.44 g of zinc nitrate and 7.35 g of sodium citrate were dissolved into 100 mL deionized water (DW) in a volumetric flask under strong stirring conditions to prepare a 0.25 M solution of zinc nitrate and sodium citrate; the stirring process continued to reach a transparent solution. 60 mL of the solution was transferred to an Erlenmeyer flask using a measuring cylinder. Subsequently, 600 mg of sodium hydroxide was added to the transparent solution and stirred for 2 h. Then, the solution was centrifuged at 9000 rpm for 15 min and washed thrice with DW and twice with ethanol to ensure the high purity of the SZN and to remove impurities.

CSZN was further synthesized using a hydrothermal method (Yang et al. 2020) where proper amounts of zinc nitrate and hexamethylenetetramine were added to DW to reach a 0.05 M solution; then, the chemicals were dissolved by stirring for 10 min. The obtained solution was mixed with 10 mL of 0.04 M sodium citrate in DW. The mixed solution was transferred to Teflon-lined autoclaves and then heated at 90 °C for 90 min. The resulting solution was centrifuged

[1] All experiments were conducted at the Islamic Azad University, South Tehran Branch, Iran, between May 2023 and March 2024. Then the modeling was developed in Sydney, Australia and Bologna, Italy.

at 9000 rpm for 15 min and washed thrice with DW and twice with ethanol to produce CSZN to remove unreacted reactants. The synthesis steps for the preparation of SZN and CSZN have been illustrated in Fig. 1.

CSZN characterization

The functional group of the synthesized CSZN was analyzed by assisting the Fourier Transform Infrared Spectroscopy (FTIR) technique. Additionally, a Field Emission Scanning Electron Microscopy (FESEM) from the TESCAN model MIRA3 was employed to evaluate the surface morphology of CSZN and compare it with SZN.

Experiments

In the first step, the desired amount of DCF (with analytical purity) was dissolved into a 2000 mL volumetric flask of double distilled water to prepare an aqueous solution of 50 mg/L DCF. To reach the ideal amount of adsorbent dosage, different quantities of SZN and CSZN (from 0.005 to 0.2 g) were chosen to dissolve in 50 mg/L DCF aqueous solution in the following conditions: contact time of 24 h (to ensure the equilibrium point was reached) and pH of 7.

Equations 1 and 2 as presented in Table 1 have been used for adsorption capacity (AC) and removal efficiency (RE), respectively, where C_0(mg/L): the concentration of DCF before the adsorption experiment, C_e(mg/L) the concentration of DCF after the adsorption experiment, V(L) the solution volume of DCF and finally W(g): dosage of SZN and CSZN.

The effects of contact time as well as pH on the removal efficiency of the adsorbent were also investigated. Here, the pH was adjusted from 3 to 11 using 0.1 M HCl or 0.1 M NaOH. To minimize any errors, all the experiments were conducted in triplicate. A

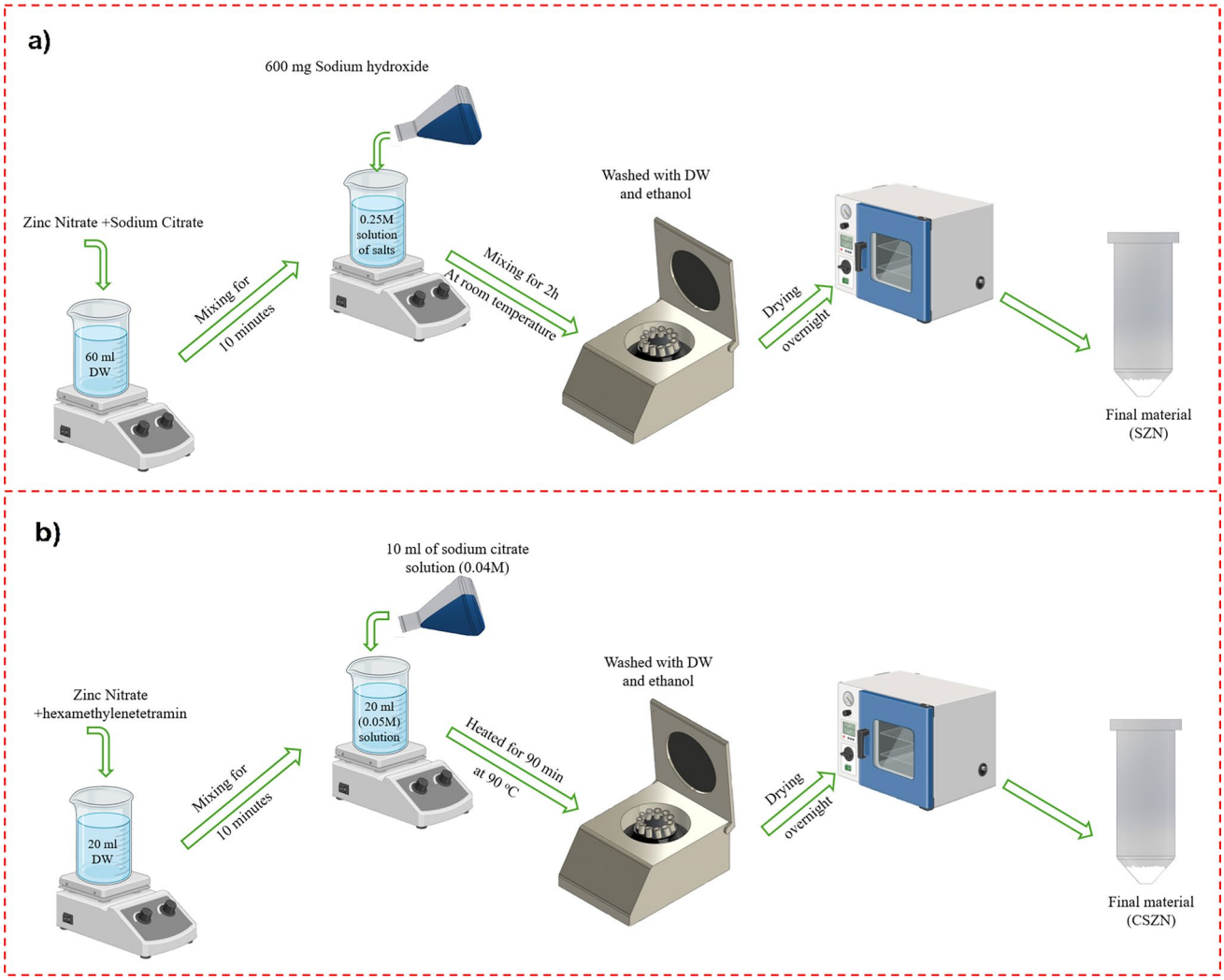

Fig. 1 Synthesis steps of SZN and CSZN

spectrophotometer (Shimadzu UV-1700) determined the DCF concentration using UV–visible spectrophotometry. Equation 3 was employed to calculate the amount of adsorbed DCF per unit mass of SZN or CSZN.

Adsorption kinetics

Three different kinetic models—pseudo-first-order, pseudo-second-order and Elovich variants—were used to fit the experimental data so that the adsorption kinetic mechanism of DCF adsorption onto SZN and CSZN could be investigated. The pseudo-first-order, pseudo-second-order and Elovich formulas are expressed in Table 2 as Eqs. 4, 5 and 6, respectively.

The parameters of kinetic models are defined as: q_e (mg/g) and q_t (mg/g) are the DCF adsorbed amount by the adsorbent to reach the equilibrium and during time t (min), respectively. For the pseudo-first-order and pseudo-second-order models, the rate constants are presented as k_1 (1/min) and k_2 (g/mg.min), respectively. α (mg.min/g) is known as the initial adsorption rate constant while β (g/mg) is the chemisorption activation energy and an indication of surface coverage extension related to the Elovich kinetic model. All the kinetic models' values are calculated based on values garnered from slopes and intercepts of the plotted data.

Equilibrium isotherms

The two-parameter models are presented in Table 3 as Eqs. 7, 8 and 9; these were used to determine the equilibrium amount of DCF adsorbed from the aqueous solution onto SZN and CSZN adsorbents. Some conventional proposals helping to understand the adsorption mechanism and adsorbent surface heterogeneity can be made by applying isotherm models to experiment data (Zuhara et al. 2023). All experiments were carried out at a constant temperature and pH over sufficient time to ensure equilibrium was achieved.

The isotherm models' parameters are q_m (mg/g): maximum adsorption capacity in the Langmuir (Lan) model, b (1/mg): adsorption-energy-related constant for Lan model, C_e (mg/L): the equilibrium concentration of DCF in an aqueous solution, q_e (mg/g): adsorbed DCF amount after reaching equilibrium, k_f and n are the maximum adsorption capacity and empirical constant of the Freundlich (Fre) model, respectively, b_T (kJ/mol): Temkin (Tem) constant, which is linked with the heat of sorption and K_T (L/mg): the equilibrium isotherm constant of the Tem isotherm.

Multi-mechanistic approach for adsorption isotherms

Apart from the conventional modeling at which a single isotherm equation is typically employed, this study aims to advance knowledge by developing a novel technique called the multi-mechanistic method, which has been used only

Table 1 Equation of adsorption capacity, removal efficiency and q_t

Name	Equations	Equation no.	References
Adsorption capacity	$AC = \frac{(C_0 - C_e) \times V}{W}$	Equation 1	Uma Maheswari et al. (2022)
Removal efficiency	$RE(\%) = \left(\frac{C_0 - C_e}{C_e}\right) \times 100$	Equation 2	Uma Maheswari et al. (2022)
DCF removal amount	$q_t = (C_0 - C_t) \times \frac{V}{M}$	Equation 3	Costa et al.(2024)

Table 2 Adsorption kinetic models

Kinetic model	Equations	Equation no.	Refernces
Pseudo-first-order	$log(q_e - q_t) = logq_e - \frac{k_1}{2.303}t$	Equation 4	Tawfik and Eltabey (2024)
Pseudo-second-order	$\frac{t}{q_t} = \frac{1}{k_2 q_e^2} + \frac{t}{q_e}$	Equation 5	Ho and McKay (1999)
Elovich	$q_t = \frac{1}{\beta} ln(\alpha\beta) + \frac{1}{\beta} lnt$	Equation 6	Shayesteh et al. (2016)

Table 3 Adsorption isotherm models

Isotherm model	Equations	Equation no.	Ref
Langmuir (Lan)	$q_e = \frac{q_m b C_e}{1 + bC_e}$	Equation 7	Wang et al. (2025)
Freundlich (Fre)	$q_e = k_f C_e^{1/n}$	Equation 8	Mani et al. (2023)
Temkin (Tem)	$q_e = \frac{RT}{b_T} ln(K_T C_e)$	Equation 9	Miraboutalebi et al. (2017)

rarely (Alyasi et al. 2021; Fritz and Schlünder 1981; McKay and Al-Duri 1991; McKay and Porter 1997). It is assumed that DCF adsorption onto CSZN follows a two-step adsorption process, and the steps can be modeled using the Fre isotherm. All experimental data from the adsorption experiments were divided into two main sections, and each of them was modeled by the Fre isotherm. In order to eliminate the linearization error, the Fre isotherm constants were calculated using the nonlinear regression method. Moreover, an Excel spreadsheet was employed to optimize data points on the stages of adsorption.

Figure 2 depicts a schematic description of the devised model. It is evident that the first adsorption section can be addressed as a major adsorption step and the maximum adsorption capacity q_e in section one has been defined as q_{s1}. Accordingly, the q_{s2} has been defined from q_{s1} to the maximum available capacity of DCF adsorption from an aqueous solution onto CSZN. The relationship between q_{sTotal}, q_{s1} and q_{s2} is as follows:

$$q_{s_{Total}} = q_{s_1} + q_{s_2} \tag{10}$$

Thus, by using the Fre equation, q_{s1} and q_{s2} will be written as $q_{e_1} = k_{f_1} C_e^{1/n_1}$ and $q_{e_2} = k_{f_2} C_e^{1/n_2}$. When C_e is at its highest value in stage 1 and stage 2 of the adsorption process, q_{e1} and q_{e2} are defined as q_{s1} and q_{s2} (Alyasi et al. 2021).

During the next step of the modeling, these Fre isotherms were fitted by the nonlinear regression technique using Lan, Sips (SIP) and Redlich Peterson (RP) isotherm equations. Different and possible combinations of SIP, RP and Lan isotherms models based on a multi-mechanistic approach are presented in Table 4.

The equations depicted in Table 4 were applied, and q_{sTotal} was determined through the utilization of experimental data. This process involved employing a nonlinear method in Excel spreadsheet for resolution purposes. The Sum of Squares Error (SSE) function served as the chosen error metric to determine the best fitting model (Al-Musawi et al. 2022).

$$SSE = \sum_{n=1}^{n} \left(q_{e_{Calculated}} - q_{e_{Experimental}} \right)^2 \tag{20}$$

where the value of $q_{e,Calculated}$ originates from the multi-mechanistic isotherm models, and $q_{e,Experimental}$ is derived from the laboratory experiments using Eq. 3.

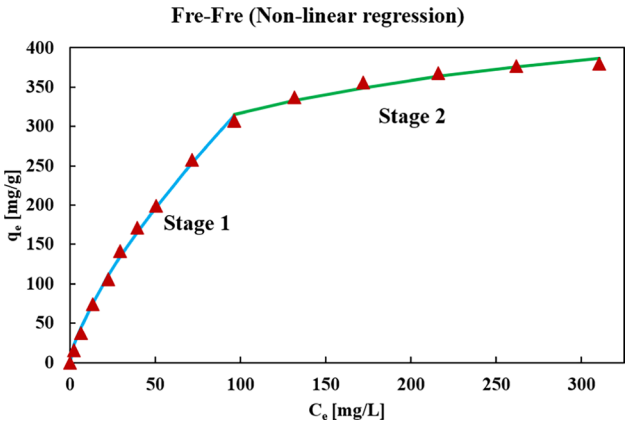

Fig. 2 Two-stage non-linear Fre model for DCF adsorption onto CSZN

Table 4 Multi-mechanistic isotherms models

Isotherm model		Equations	Equation no.	References
Lan	Lan	$q_e = \frac{q_{s1}K_{L1}C_e}{1+K_{L1}C_e} + \frac{q_{s2}K_{L2}C_e}{1+K_{L2}C_e}$	Equation 11	Alyasi et al. (2021), Hu et al. (2023), Murphy et al. (2023)
Sip	Sip	$q_e = \frac{q_{s1}K_{S1}C_e^{\alpha 1}}{1+K_{S1}C_e^{\alpha 1}} + \frac{q_{s2}K_{S2}C_e^{\alpha 2}}{1+K_{S2}C_e^{\alpha 2}}$	Equation 12	
RP	RP	$q_e = \frac{q_{s1}K_{R1}C_e}{1+K_{R1}C_e^{\beta 1}} + \frac{q_{s2}K_{R2}C_e}{1+K_{R2}C_e^{\beta 2}}$	Equation 13	
Lan	Sip	$q_e = \frac{q_{s1}K_{L1}C_e}{1+K_{L1}C_e} + \frac{q_{s2}K_{S2}C_e^{\alpha 2}}{1+K_{S2}C_e^{\alpha 2}}$	Equation 14	
Sip	Lan	$q_e = \frac{q_{s1}K_{S1}C_e^{\alpha 1}}{1+K_{S1}C_e^{\alpha 1}} + \frac{q_{s2}K_{L2}C_e}{1+K_{L2}C_e}$	Equation 15	
Lan	RP	$q_e = \frac{q_{s1}K_{L1}C_e}{1+K_{L1}C_e} + \frac{q_{s2}K_{R2}C_e}{1+K_{R2}C_e^{\beta 2}}$	Equation 16	
RP	Lan	$q_e = \frac{q_{s1}K_{R1}C_e}{1+K_{R1}C_e^{\beta 1}} + \frac{q_{s2}K_{L2}C_e}{1+K_{L2}C_e}$	Equation 17	
RP	Sip	$q_e = \frac{q_{s1}K_{R1}C_e}{1+K_{R1}C_e^{\beta 1}} + \frac{q_{s2}K_{S2}C_e^{\alpha 2}}{1+K_{S2}C_e^{\alpha 2}}$	Equation 18	
Sip	RP	$q_e = \frac{q_{s1}K_{S1}C_e^{\alpha 1}}{1+K_{S1}C_e^{\alpha 1}} + \frac{q_{s2}K_{R2}C_e}{1+K_{R2}C_e^{\beta 2}}$	Equation 19	

Results and discussion

Characterization

The FTIR spectroscopic analysis, which is presented in Fig. 3a, explains the characteristics of both SZN (a) and CSZN (b) within the 4000–450 cm^{-1} range. The same functional groups in both samples can be seen from the spectra, emphasizing the solid properties of the materials under different preparation methods. Major peaks that can be observed in both SZN and CSZN spectra occur at 456, 620, 658, 924, 1018, 1108, 1250, 1416, 1576, and 3438 cm^{-1}. Particularly, the existence of Zn–O stretch vibrations that were verified by a peak at 456 cm^{-1} can confirm ZnO formation (Abomuti et al. 2021). The presence of additional organic functional groups, such as =C–H, C–O, and C=O, likely results from residual synthesis agents and does not affect the main ZnO phase, as confirmed by the strong Zn–O peak and SEM images. Furthermore, the presence of O–H bending vibrations can be found at 620 cm^{-1}, while the =C–H bending vibrations appear as distinct bands at 658 and 924 cm^{-1}. Peaks at 1018 and 1108 cm^{-1} indicate the stretching vibration of C–O bonds. Additional bands are detected at 1416 cm^{-1}, which symbolizes C–H bending vibrations, and 1576 cm^{-1}, which confirms the existence of the C=O amide II group. The presence of free water, indicated by the bending vibration of H–O–H bonds, is suggested by the broad band detected at 3438 cm^{-1} (Abomuti et al. 2021; Alamdari et al. 2020).

Furthermore, the topographical features of SZN and its clew-shaped counterpart, CSZN, were studied by using a scanning electron microscope (SEM), and the outcomes are shown in Fig. 3b–f. The surface of SZN demonstrated very little porosity. However, CSZN revealed a lot of micro and macropores with many uneven and fractured surfaces, making it a better candidate for the adsorption process. It should be clarified that the clew-shaped CSZN is not composed of distinct threads or wires but is instead characterized by an irregularly rough, porous, ball-like aggregate structure that creates more voids and accessible sites for adsorption. The developed preparation method resulted in a major shift in morphology and structure, as seen by the outstandingly increased surface roughness and irregularity of CSZN compared to SZN.

Adsorption capacity and removal efficiency

Based on the experimental data, the adsorption capacity and removal efficiency were calculated for different adsorbent dosages, and the results are shown in Fig. 4a and b. As demonstrated, the adsorption capacity diminishes as the adsorbent dosage increases because the total number of active

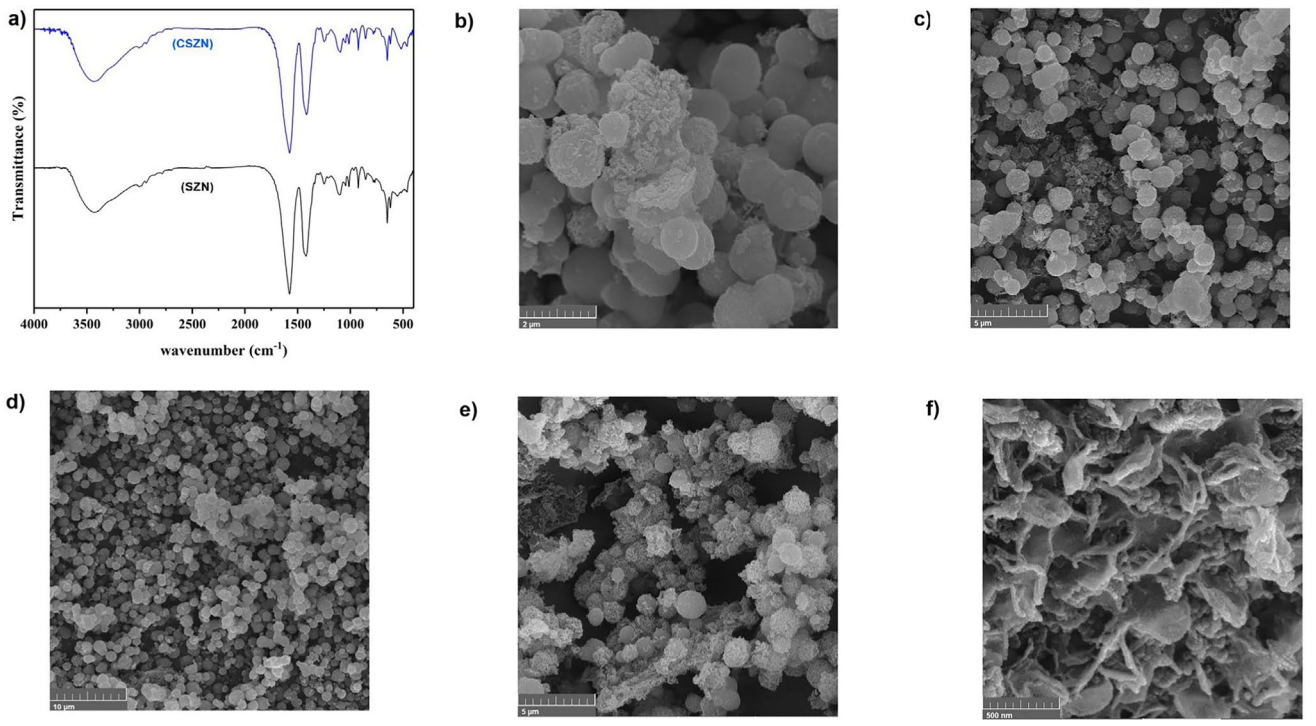

Fig. 3 Characterization: **a** FTIR spectra of SZN and CSZN, **b** SEM image of SZN (2 µm), **c** SEM image of SZN (5 µm), **d** SEM image of SZN (10 µm), **e** SEM image of CSZN (5 µm), **f** SEM image of CSZN (500 nm)

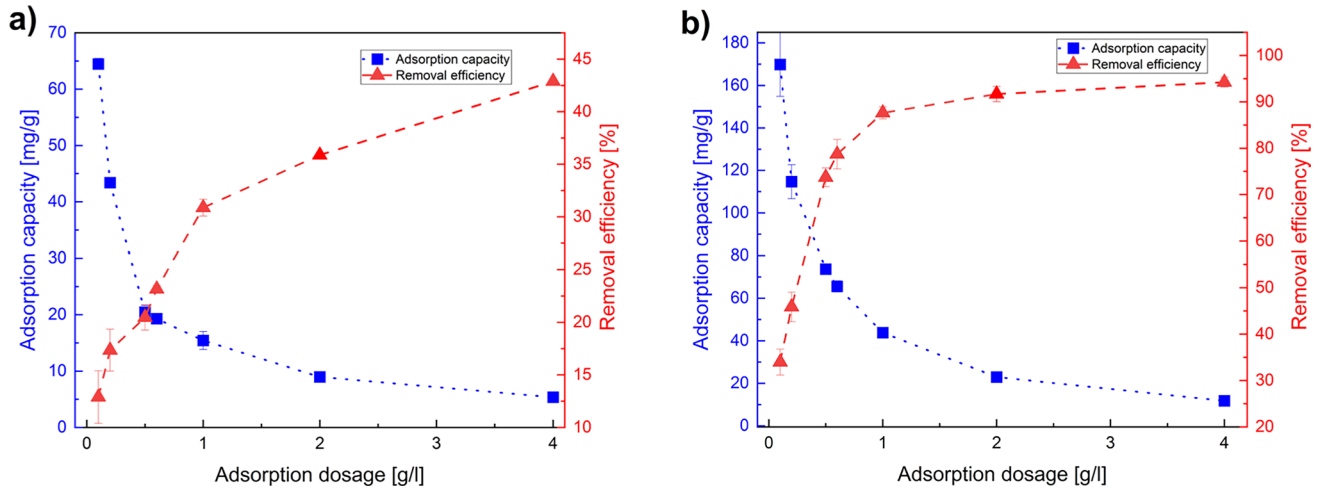

Fig. 4 Adsorption capacity and removal efficiency trends for (a) SZN (b) CSZN in terms of DCF dosage at contact time: 24 h, pH: 7 and C_0: 50 mg/L

sites becomes excessive relative to the fixed amount of DCF. Furthermore higher dosages may cause particle aggregation, reducing the effective surface area and active site accessibility. Conversely, the removal efficiency increases with larger dosages, reaching an optimal plateau where nearly all target molecules are removed from the solution.

DCF removal experiments using the adsorption method

Effect of contact time on DCF removal

The effect of contact time on the adsorption process of DCF onto SZN and CSZN was plotted and shown in Fig. 5a. The adsorption behavior of DCF onto CSZN reveals a sequential two-step process. Initially, a swift adsorption phase occurs, promptly followed by a subsequent phase characterized by a slower adsorption rate.

Effect of pH on DCF removal

According to Fig. 5b, the amount of DCF removed using both SZN and CSZN adsorbents greatly depends on the pH of the aqueous solution. Lower pH values in the experiments show a stronger tendency for DCF adsorption onto SZN and CSZN.

Effect of initial concentration on DCF removal

The relationship between q_e (mg/g) and the initial DCF concentration during DCF adsorption onto CSZN and SZN is graphically shown in Fig. 5c. As the initial DCF

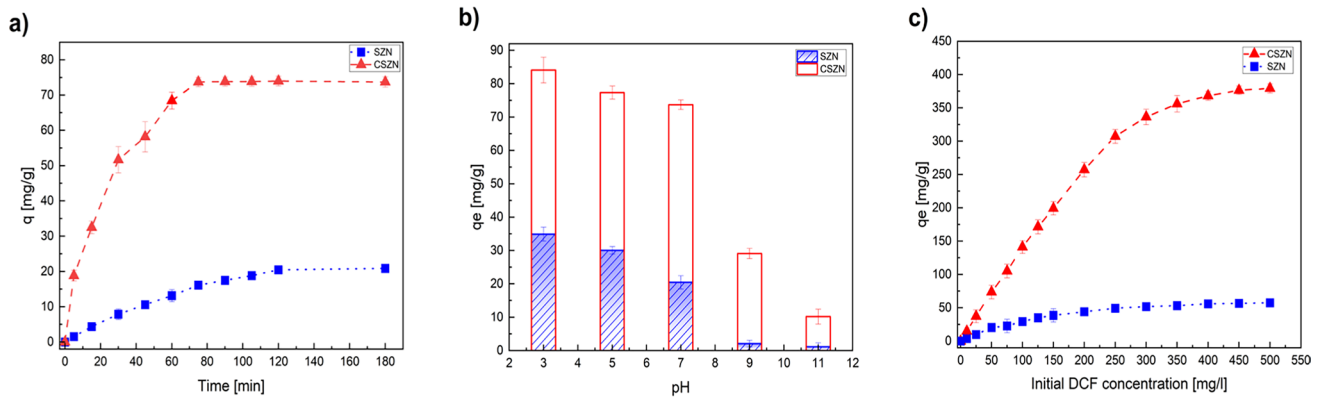

Fig. 5 **a** Contact time effect on the adsorption at pH: 7, C_0: 50 mg/L and adsorbent dosage: 0.5 g/L, **b** pH effect on the adsorption at contact time: 120 min, C_0: 50 mg/L and adsorbent dosage: 0.5 g/L, **c** Initial DCF concentration effect on the adsorption at pH:7, contact time: 120 min, C_0: 50 mg/L and adsorbent dosage: 0.5 g/L

concentration in the aqueous solution escalated, there was a corresponding increase in q_e.

Kinetics of the DCF adsorption process

The kinetic mechanisms for the adsorption of DCF onto SZN and CSZN were investigated by fitting the obtained in-lab data to the pseudo-first-order, pseudo-second-order, and Elovich kinetic models. As shown in Fig. S1a–c, in SI, the data were fitted by employing linear regression, and the constants of the models were presented using the obtained linear equations. The adsorption kinetic parameters for each kinetic model have been summarized and presented in Table 5.

Adsorption isotherm study

The experimental adsorption data at equilibrium were fitted using Lan, Fre, and Tem isotherms to model the adsorption of DCF from aqueous solution onto SZN and CSZN. The linear regression technique was employed for this purpose, and the resulting equations along with their respective R^2 values are presented in Fig. S2a–c in the SI. Furthermore, all isotherm parameters for both SZN and CSZN were computed based on the fitted data and are summarized in Table 6. A comparison of different adsorbents for DCF removal from aqueous solution based on Lan q_m, the experiment contact time, pH, and adsorbent dosage is presented in Table 7.

Table 5 Calculated parameters for kinetic models of DCF adsorption onto SZN and CSZN

Kinetic model	Model constants					
	SZN			CSZN		
Pseudo-first-order	$k_1 = 0.0302$	$q_{e,Calc.} = 32.4$	$R^2 = 0.87$	$k_1 = 0.0405$	$q_{e,Calc.} = 73.9$	$R^2 = 0.97$
Pseudo-second-order	$k_2 = 0.0002$	$q_{e,Calc.} = 44.5$	$R^2 = 0.99$	$k_2 = 0.0007$	$q_{e,Calc.} = 83.4$	$R^2 = 0.99$
Elovich	$\alpha = 1.047$	$\beta = 0.166$	$R^2 = 0.92$	$\alpha = 8.829$	$\beta = 0.051$	$R^2 = 0.96$

Table 6 Calculated parameters for isotherm models of DCF adsorption onto SZN and CSZN

Isotherm model	Model constant					
	SZN			CSZN		
Langmuir (Lan)	$q_m = 87.72$	$b = 0.006$	$R^2 = 0.99$	$q_m = 555.56$	$b = 0.011$	$R^2 = 0.99$
Freundlich (Fre)	$k_f = 1.59$	$n = 1.61$	$R^2 = 0.94$	$k_f = 12.28$	$n = 1.51$	$R^2 = 0.94$
Temkin (Tem)	$K_T = 9.06$	$b_T = 166.58$	$R^2 = 0.97$	$K_T = 4.22$	$b_T = 27.14$	$R^2 = 0.95$

Table 7 Comparison of maximum adsorption capacity, based on Langmuir isotherm, of CSZN and different adsorbents for DCF removal from aqueous solution

Adsorbent	$q_{m,Lan}$ (mg/g)	Time (min)	Adsorbent dosage (g/L)	pH	References
CSZN	555.6	120	0.5	7	This work
P(ECH- DETA) hydrogel	540	150	0.5	NC[1]	Jiang et al. (2022)
COF TAPT- DVA-NH_2	398.4	60	0.34	NC	Xiao et al. (2024)
HC-10	376.2	300	0.2	5.6	Chatir et al. (2023)
M–TDiCOF	359.41	180	0.08	NC	Lin et al. (2024)
TCPP@UiO-66/PAN	202	120	–	NC	Gao et al. (2024)
MWCNT@OH-COOH-Fe	174.1	360	1.5	NC	Costa et al. (2024a, b)
Zeolite treated with nitric acid	85.9	120	0.4	6	Peñafiel et al. (2024)
COF TAPT- DVA	64.4	60	0.34	NC	Xiao et al. (2024)
Fe_3O_4-ZnO/DES-modified rice husk	24.33	360	2	2	(Hinsene et al. 2024)
Chitosan-modified fibrous Silica KCC-1	17.24	40	1	4	Lai et al. (2023)
MPDA-CS	3.25	1440	25	7	Sun et al. (2022)

[1]Not Controlled

Table 8 Fre isotherm parameters calculated based on nonlinear regression

Freundlich (Fre)	Model constant		
	CSZN		
First Stage	$k_{f1} = 11.92$	$\frac{1}{n_1} = 0.72$	$q_{s_1} = 314.33$
Second Stage	$k_{f2} = 142.35$	$\frac{1}{n_2} = 0.17$	$q_{s_2} = 71.39$

Multi-mechanistic approach for isotherm modeling of DCF adsorption onto CSZN

Two distinct multi-mechanistic approaches were implemented to model a two-step adsorption process of DCF onto CSZN. The obtained Fre isotherm parameters are tabulated in Table 8. The resulting computed parameters for both multi-mechanistic approaches are presented in Tables S2 and S3 in the SI, respectively. Figures 6a–i and 7a–i graphically illustrate the curves obtained from both multi-mechanistic approaches.

Discussion

Characterization

The adsorption properties of materials are influenced not only by their chemical composition but also significantly by their physical structure and surface morphology. Although FTIR results indicated similar functional groups for both adsorbents, notable differences were observed in their adsorption capacities. Specifically, the unique clew-shaped morphology of CSZN created more accessible active sites and enhanced surface roughness, directly contributing to its higher adsorption capacity for DCF. This clear correlation between morphology and adsorption properties underscores

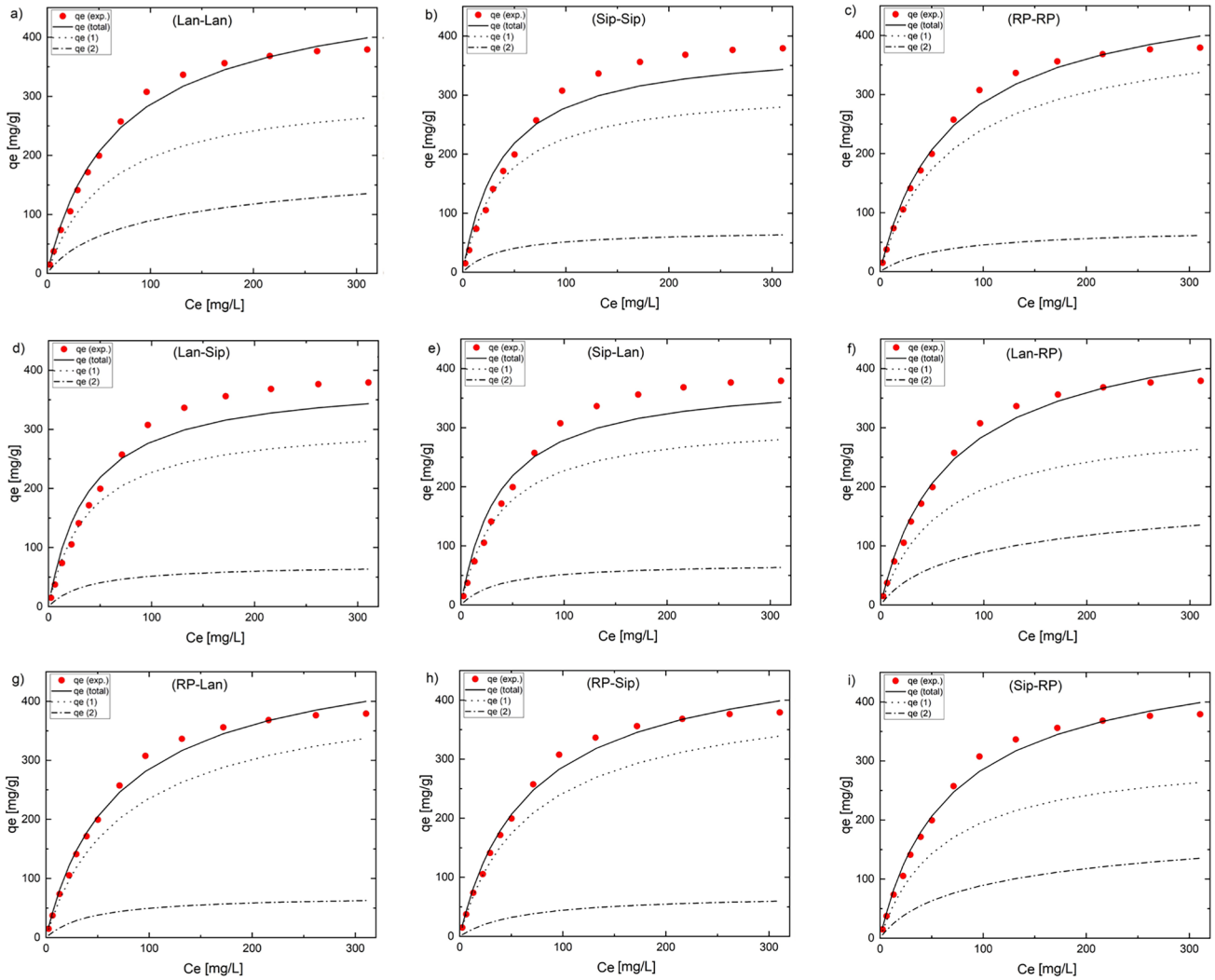

Fig. 6 q_e versus C_e curves based on a multi-mechanism approach for DCF adsorption onto CSZN using two-stage Fre isotherm

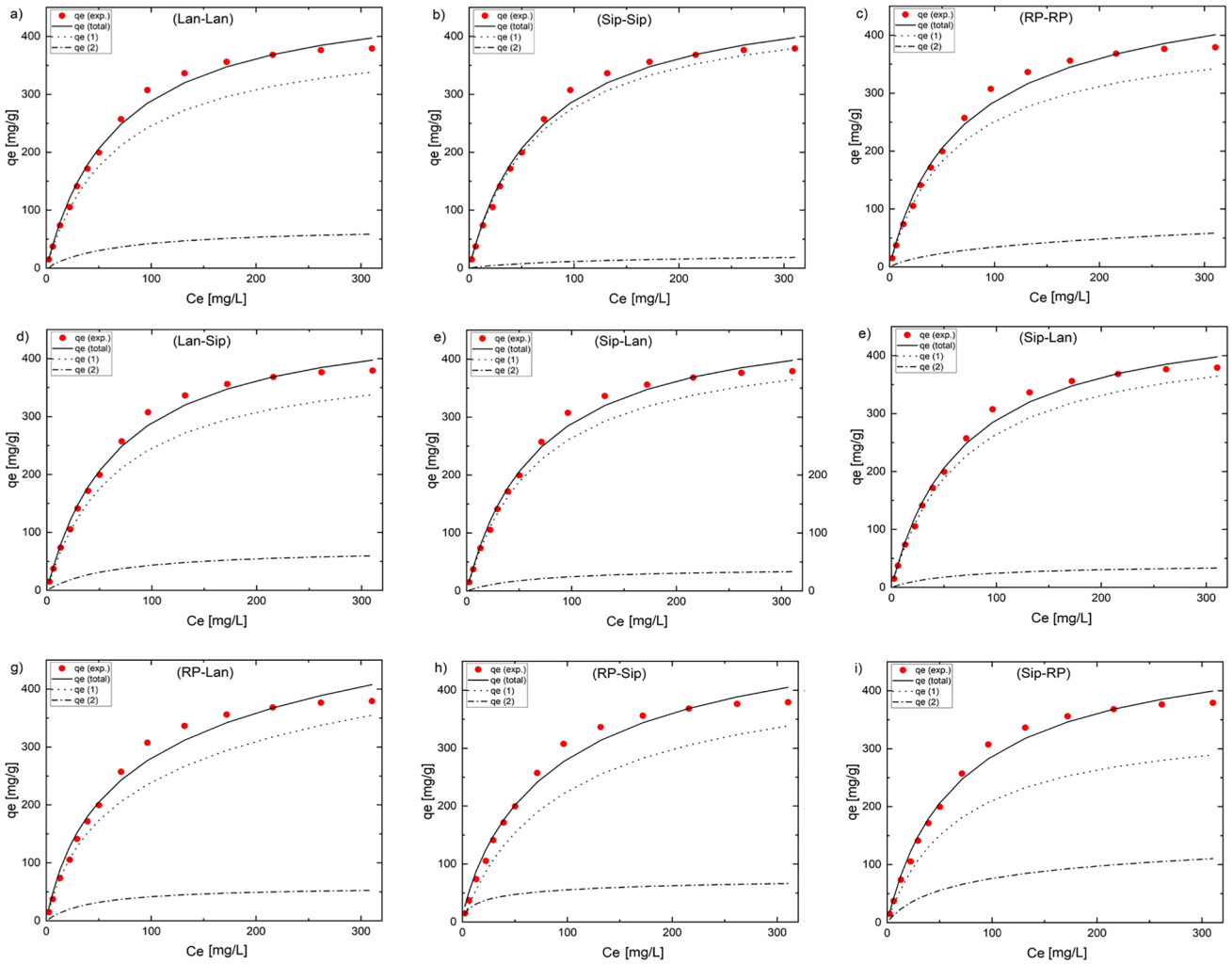

Fig. 7 q_e versus C_e curves based on the multi-mechanism approach for DCF adsorption onto CSZN using the total capacity of adsorption

the crucial role of structural modification in optimizing adsorbent performance. It is worth noting that owing to the newly gained uneven structure and surface, which makes more favorable sites for adsorption, the inclusion of clew-shaped features resulted in greater surface area and increased adsorption capacity. This change introduces CSZN as a potential DCF adsorbent that works perfectly. Therefore, the results strongly indicate the successful enhancement of adsorption properties through morphological engineering of the CSZN adsorbent.

Adsorption capacity and removal efficiency

The trend emphasizes the balance between maximizing removal efficiency and achieving high capacity per unit mass of adsorbent. Thus, selecting an optimal adsorbent dosage is crucial to achieving cost-effective and efficient removal of DCF. These findings suggest that practical applications should consider this trade-off to optimize adsorbent utilization.

From the adsorption capacity perspective, it is worth noting that the remarkably enhanced adsorption capacity of CSZN is predominantly due to its distinct clew-shaped morphology, which was successfully achieved through the modified synthesis approach implemented in this study. As demonstrated by the SEM images in Fig. 3a–f, CSZN exhibits a highly rough, high surface, and clew-like structure, whereas SZN has a relatively smooth and smaller surface. This structural difference creates more accessible active sites and provides more pathways for DCF molecules to diffuse and interact with the adsorbent surface. Additionally, the FTIR analysis confirms that the functional groups in SZN and CSZN are qualitatively the same, which means that the improved performance is not due to a change in chemical functional groups, but rather due to the

enhanced physical surface characteristics and the greater heterogeneity of the CSZN surface.

Furthermore, the faster adsorption kinetics observed for CSZN, compared to SZN, support this interpretation. A more irregular and open morphology reduces diffusion limitations and allows DCF molecules to reach active sites more efficiently. In summary, the improved adsorption capacity is mainly interpreted as a result of the structural and morphological advantages of the clew-shaped ZnO, which increase the number of available adsorption sites and improve mass transfer.

Influence of adsorption conditions on DCF removal capacity

By evaluating the adsorption of DCF onto SZN and CSZN, it becomes evident that the q_t (mg/g) for DCF removal from aqueous solutions by CSZN significantly exceeds that of SZN under an identical operating condition. Notably, CSZN adsorbed 250% more DCF than SZN, emphasizing the superior adsorption capacity of CSZN. The time to reach the second adsorption phase for CSZN was also faster (only 80 min compared to 120 min for SZN). The faster and higher increase can be attributed to a much greater surface area and, consequently, an increase in the number of available active sites in CSZN for adsorption. Moreover, the clew-shaped, irregular, and porous surface of CSZN provides more accessible sites, shorter diffusion pathways, and reduced mass transfer resistance, enabling DCF molecules to be adsorbed more quickly. In this way, a noticeably higher capacity for DCF adsorption onto the adsorbent was possible with CSZN compared to SZN. Furthermore, a reduction in the adsorption rate for the second phase can be attributed to forming a DCF monolayer on the active CSZN sites.

The pH-dependent adsorption behavior of DCF can be explained by its chemical structure, particularly the presence of a carboxylic acid group. DCF is a weakly acidic pharmaceutical compound whose ionization state varies with pH. At lower pH values, DCF predominantly exists in its neutral (protonated) form, which facilitates stronger interactions with adsorbent surfaces. In contrast, at higher pH levels, DCF becomes deprotonated and exists as an anionic species, which can lead to electrostatic repulsion from negatively charged adsorbent surfaces and consequently reduce adsorption capacity. This effect is evident for CSZN, where the formation of DCF anions at higher pH values increases repulsive forces, resulting in a sharp drop in adsorption capacity from 84 mg/g at pH 3 to approximately 10 mg/g at pH 11.

Regarding the initial DCF concentration, the increase in adsorption capacity (q_e) can be attributed to the greater driving force for mass transfer from the solution to the adsorbent surface. Moreover, the experimental data clearly demonstrate significantly higher q_e values for CSZN compared to SZN at equivalent initial concentrations. This finding further confirms the superior affinity and efficiency of CSZN for DCF adsorption, highlighting its potential as an effective adsorbent for practical water treatment applications.

Comprehensive kinetic and multi-mechanistic isotherm analysis

The calculated R^2 values strongly suggest that the Lan isotherm model effectively predicts DCF adsorption onto SZN and CSZN. Specifically, the R^2 values were determined to be 0.99 for both SZN and CSZN when the Lan isotherm model was applied to predict the adsorption behavior. This high R^2 means the model has a robust prediction capability and suggests that the adsorption process can be well-described by the formation of a monolayer. In other words, it can be said that the sorbent surface is covered by a single layer of adsorbates. Additionally, a homogeneous distribution of activity on the adsorbents' surfaces, as well as an even presence of active sites throughout the surface, can be assumed.

In the multi-mechanistic isotherm modeling, as explained in "Multi-mechanistic approach for adsorption isotherms" section, the experimental dataset was intentionally partitioned into two primary categories to produce the most accurate analysis. The Fre isotherm model was used for each category to determine the values of the adsorption capacities, namely q_{s1} and q_{s2}. To avoid linearization errors, a non-linear regression technique was employed, resulting in the determination of kinetic constants k_{f1}, k_{f2}, as well as equilibrium parameters n_1 and n_2. Then, combinations of Lan, SIP, and RP isotherm models functioned to explain the DCF adsorption behavior onto CSZN, using predetermined values of $q_{s1} = 314.33$ (mg/g) and $q_{s2} = 71.39$ (mg/g). The complex modeling procedure was carried out by using an Excel spreadsheet for a non-linear regression method. Interestingly, the results showed that multi-mechanism modeling produced a much better fit and presented a superior ability to predict the adsorption data in contrast to the use of a single isotherm model mentioned previously. Multi-mechanism modeling revealed that RP-RP is the best model with a lower SSE of 2193 compared to single-isotherm Lan with SSE of 5505. This significant improvement confirms the necessity of adopting multi-mechanistic approaches for accurately capturing certain adsorption processes, especially when complex mechanisms or multiple adsorption stages are involved.

The second multi-mechanistic approach was designed to avoid using fixed values for q_{s1} and q_{s2} during the adsorption modeling. In this different scheme, again, various combinations of Lan, SIP, and RP isotherm models were used, as well as a nonlinear regression method helped by what was documented on an Excel spreadsheet. Nonlinear regression techniques were employed to determine the isotherm model

parameters for each combined equation. The results of the modeling showed that the Lan-Lan isotherm model had better predictive power when it came to DCF adsorption onto CSZN. In comparison to the first multi-mechanism technique, the calculated SSE for Lan-Lan was obtained (1735), which significantly decreased and indicated a reduction of approximately 20%. This further improvement reinforces the flexibility and robustness of the multi-mechanistic approach, demonstrating its superiority over conventional single-model fitting, and highlights its potential as a reliable method for interpreting complex adsorption data.

The aforementioned methodology emphasizes two points: the adaptability of the multi-mechanistic modeling structure and the effectiveness of the Lan-Lan isotherm model in representing the complexities of the DCF adsorption process on CSZN. The advantage of using the Lan-Lan (multi-mechanistic) isotherm model over a single Langmuir model lies in its ability to account for multiple adsorption behaviors occurring within a single system. Most practical adsorbents, including CSZN, feature heterogeneous surfaces with a variety of adsorption sites and energies. This leads to a typical two-stage process: an initial rapid uptake on high-energy, easily accessible sites, followed by a slower phase as adsorption shifts to less accessible or lower-energy regions. The Lan-Lan model effectively divides the process into these distinct stages, enabling each to be described with its own set of parameters. This approach not only improves the model fit but also provides a more realistic and accurate interpretation of how adsorption progresses on complex materials.

This advanced multi-mechanistic modeling provides deeper insights and stronger predictive capabilities compared to traditional single-model approaches. In reality, actual adsorption systems seldom follow an idealized, single-step mechanism. Instead, they involve dynamic transitions such as surface adsorption, pore filling, or multilayer interactions, which are especially common in porous and heterogeneous materials like CSZN. By modeling each phase separately within the Lan-Lan framework, the approach delivers more reliable design parameters and improves understanding of both adsorption capacity and the nature of interactions. Consequently, it becomes a valuable tool for optimizing adsorbent performance in environmental remediation applications.

Conclusion

The main goals of this study were synthesis and evaluation of a new adsorbent, CSZN as well as introducing a new model using a multi-mechanism modeling approach. CSZN exhibited a significantly better adsorption capability than SZN during different adsorption experiments for DCF removal from an aqueous solution. The impacts of different operational parameters on the DCF's adsorption process on SZN and CSZN were investigated. These parameters included the initial concentration of DCF, the pH of the aqueous solution as well as the contact time.

Pseudo-first-order, pseudo-second-order, and Elovich equations were employed as kinetic models to understand and elucidate the kinetics of the adsorption process. Furthermore, the three most used isotherm models were employed to study the adsorption behavior of DCF onto SZN and CSZN. The research then used two different multi-mechanistic techniques to improve the isotherm model's predictive power for DCF adsorption onto CSZN. Based on the modeling results, the Lan-Lan isotherm model had the smallest SSE, which emphasizes having a better ability to predict the adsorption behavior of CSZN. This outcome highlights: firstly, how well the multi-mechanistic method improves prediction accuracy; and secondly, how well the Lan-Lan isotherm model foretells the behavior of the DCF adsorption process onto CSZN. In summary, this study demonstrates the potential of CSZN in effectively removing DCF from aqueous environments and the efficacy of the offered multi-mechanistic approach in modeling the adsorption process of pharmaceutical contaminant removal in wastewater.

Supplementary Information The online version contains supplementary material available at https://doi.org/10.1007/s13762-025-06751-4.

Acknowledgements The authors would like to thank H. Shayesteh and M. Peydayesh for their guidance during this research. The 2nd author acknowledged the International Research Training Program Scholarship (IRTP) from the University of Technology Sydney (UTS).

Author contributions Nima Allahgholi: Conceptualization, methodology, experimental work, writing, visualization, reviewing and editing. Seyed Mohammadreza Miraboutalebi: Conceptualization, methodology, modeling, writing original draft, visualization, reviewing and editing. Mina Sohrabi: Conceptualization, methodology, writing, reviewing and editing. Tien Vinh Nguyen: Supervision, reviewing and editing. Saravanamuthu Vigneswaran: Supervision, reviewing and editing. Gordon McKay: Supervision, reviewing and editing.

Funding Open Access funding enabled and organized by CAUL and its Member Institutions.

Declarations

Conflict of interest The authors declare that they have no relevant financial interests or personal relationships that could have been recognized as influencing the research presented in this paper.

References

Abomuti MA, Danish EY, Firoz A, Hasan N, Malik MA (2021) Green synthesis of zinc oxide nanoparticles using *Salvia officinalis* leaf extract and their photocatalytic and antifungal activities. Biology 10(11):1075

Ahsani-Namin Z, Norouzbeigi R, Shayesteh H (2022) Green mediated combustion synthesis of copper zinc oxide using *Eryngium planum* leaf extract as a natural green fuel: excellent adsorption capacity towards Congo red dye. Ceram Int 48(14):20961–20973. https://doi.org/10.1016/j.ceramint.2022.04.090

Al-Musawi TJ, McKay G, Kadhim A, Joybari MM, Balarak D (2022) Activated carbon prepared from hazelnut shell waste and magnetized by Fe_3O_4 nanoparticles for highly efficient adsorption of fluoride. Biomass Convers Biorefin. https://doi.org/10.1007/s13399-022-02593-z

Alamdari S, Sasani Ghamsari M, Lee C, Han W, Park H-H, Tafreshi MJ, Afarideh H, Ara MHM (2020) Preparation and characterization of zinc oxide nanoparticles using leaf extract of *Sambucus ebulus*. Appl Sci 10(10):3620

Alessandretti I, Rigueto CVT, Nazari MT, Rosseto M, Dettmer A (2021) Removal of diclofenac from wastewater: a comprehensive review of detection, characteristics and tertiary treatment techniques. J Environ Chem Eng 9(6):106743. https://doi.org/10.1016/j.jece.2021.106743

Alharthi FA, Alghamdi AA, Al-Zaqri N, Alanazi HS, Alsyahi AA, Marghany AE, Ahmad N (2020) Facile one-pot green synthesis of Ag–ZnO nanocomposites using potato peeland their Ag concentration dependent photocatalytic properties. Sci Rep 10(1):20229. https://doi.org/10.1038/s41598-020-77426-y

Almasri DA, Saleh NB, Atieh MA, McKay G, Ahzi S (2019) Adsorption of phosphate on iron oxide doped halloysite nanotubes. Sci Rep 9(1):3232. https://doi.org/10.1038/s41598-019-39035-2

Alyasi H, Mackey H, McKay G (2021) Novel model analysis for multimechanistic adsorption processes: case study: cadmium on nanochitosan. Sep Purif Technol 274:117925. https://doi.org/10.1016/j.seppur.2020.117925

Araujo LA, Bezerra CO, Cusioli LF, Rodríguez MT, Gomes RG, Bergamasco R (2021) Diclofenac adsorption using a low-cost adsorbent derived from *Guazuma ulmifolia* Lam. fruit via chemical and thermal treatment. J Environ Chem Eng 9(6):106629. https://doi.org/10.1016/j.jece.2021.106629

Areeb A, Yousaf T, Murtaza M, Zahra M, Zafar MI, Waseem A (2021) Green photocatalyst Cu/NiO doped zirconia for the removal of environmental pollutants. Mater Today Commun 28:102678. https://doi.org/10.1016/j.mtcomm.2021.102678

Carmo Jd, Justino NM, Matias MS, Puerari RC, Matias WG, Ladner D, Vicentini DS, Nagel Hassemer ME (2022) Membrane adsorption with polyacrylonitrile prepared with superfine powder-activated carbon, case study: separation process applied in water treatment containing diclofenac. Environ Technol 43(4):478–488. https://doi.org/10.1080/09593330.2020.1793006

Chatir EM, El Hadrami A, Ojala S, Brahmi R (2023) Thermal treatment of H3PO4-impregnated hydrochar under controlled oxygen flows for producing materials with tunable properties and enhanced diclofenac adsorption. Sustain Chem Pharm 34:101164. https://doi.org/10.1016/j.scp.2023.101164

Chyoshi B, Gomes Coelho LH, García J, Subtil EL (2022) Fate and removal of emerging contaminants in anaerobic fluidized membrane bioreactor filled with thermoplastic gel as biofilm support. Chemosphere 300:134557. https://doi.org/10.1016/j.chemosphere.2022.134557

Costa HPdS, Duarte EDV, da Silva MGC, Vieira MGA (2024a) Adsorption of diclofenac and losartan using multi-walled carbon nanotubes functionalized with iron nanoparticles via the green route: equilibrium, thermodynamics, and machine learning studies. J Water Process Eng 58:104923. https://doi.org/10.1016/j.jwpe.2024.104923

Costa HPS, Duarte EDV, da Silva FV, da Silva MGC, Vieira MGA (2024b) Green synthesis of carbon nanotubes functionalized with iron nanoparticles and coffee husk biomass for efficient removal of losartan and diclofenac: adsorption kinetics and ANN modeling studies. Environ Res 251:118733. https://doi.org/10.1016/j.envres.2024.118733

de Souza dos Santos GE, Ide AH, Duarte JLS, McKay G, Silva AOS, Meili L (2020) Adsorption of anti-inflammatory drug diclofenac by MgAl/layered double hydroxide supported on *Syagrus coronata* biochar. Powder Technol 364:229–240. https://doi.org/10.1016/j.powtec.2020.01.083

Dekkouche S, Morales-Torres S, Ribeiro AR, Faria JL, Fontàs C, Kebiche-Senhadji O, Silva AMT (2022) In situ growth and crystallization of TiO2 on polymeric membranes for the photocatalytic degradation of diclofenac and 17α-ethinylestradiol. Chem Eng J 427:131476. https://doi.org/10.1016/j.cej.2021.131476

Devaisy S, Kandasamy J, Nguyen TV, Johir MAH, Ratnaweera H, Vigneswaran S (2022) Comparison of membrane-based treatment methods for the removal of micro-pollutants from reclaimed water. Water 14(22):3708

Dzimitrowicz A, Terefinko D, Bielawska-Pohl A, Motyka-Pomagruk A, Jamroz P, Cyganowski P, Lenard K, Pohl P, Klimczak A, Caban M (2024) Biosafe removal of diclofenac from wastewaters by a continuous-flow mode cold atmospheric pressure plasma system. J Environ Chem Eng 12(1):111598. https://doi.org/10.1016/j.jece.2023.111598

Elshikh MS, Hussein DS, Al-khattaf FS, Rasheed El-Naggar RA, Almaary KS (2022) Diclofenac removal from the wastewater using activated sludge and analysis of multidrug resistant bacteria from the sludge. Environ Res 208:112723. https://doi.org/10.1016/j.envres.2022.112723

Fritz W, Schlünder EU (1981) Competitive adsorption of two dissolved organics onto activated carbon—I: Adsorption equilibria. Chem Eng Sci 36(4):731–741. https://doi.org/10.1016/0009-2509(81)85088-9

Gao Y, Cheng T, Zhao F, Huang G, Bi J (2024) A hybrid linker-MOF fibrous composite for efficient diclofenac removal and self-cleaning. Sep Purif Technol 337:126260. https://doi.org/10.1016/j.seppur.2023.126260

Hinsene H, Bhawawet N, Imyim A (2024) Rice husk biochar doped with deep eutectic solvent and Fe3O4/ZnO nanoparticles for heavy metal and diclofenac removal from water. Sep Purif Technol 339:126638. https://doi.org/10.1016/j.seppur.2024.126638

Ho YS, McKay G (1999) Pseudo-second order model for sorption processes. Process Biochem 34(5):451–465. https://doi.org/10.1016/S0032-9592(98)00112-5

Hu Q, Lan R, He L, Liu H, Pei X (2023) A critical review of adsorption isotherm models for aqueous contaminants: curve characteristics, site energy distribution and common controversies. J Environ Manage 329:117104. https://doi.org/10.1016/j.jenvman.2022.117104

Jiang X, Ding W, Li H, Zhang Z, Zhong Z, Liu H, Zheng H (2022) Facile synthesis of poly(epichlorohydrin-diethylenetriamine) hydrogel for highly selective diclofenac sodium removal. Sep Purif Technol 283:120215. https://doi.org/10.1016/j.seppur.2021.120215

Kandaswamy K, Guru A, Panda SP, Antonyraj APM, Kari ZA, Giri J, Almutairi BO, Arokiyaraj S, Malafaia G, Arockiaraj J (2024)

Polystyrene nanoplastics synergistically exacerbate diclofenac toxicity in embryonic development and the health of adult zebrafish. Comp Biochem Physiol C Toxicol Pharmacol 281:109926. https://doi.org/10.1016/j.cbpc.2024.109926

Lai LW, Teh LP, Timmiati SN, Kamarudin NHN, Setiabudi HD (2023) A sustainable solution for diclofenac adsorption: Chitosan-modified fibrous silica KCC-1 adsorbent. J Environ Chem Eng 11(6):111295. https://doi.org/10.1016/j.jece.2023.111295

Lin Z, Jin Y, Xiao Z, Li Y, Lin Y, Chen Z, Zhuang X, Mo P, Liu Y, Chen P, Lv W, Liu G (2024) Comprehensive insights into non-steroidal anti-inflammatory drugs adsorption by magnetic ionic covalent organic framework: kinetics, isotherms, and mechanisms. Sep Purif Technol 339:126628. https://doi.org/10.1016/j.seppur.2024.126628

Mani D, Elango D, Priyadharsan A, Al-Humaid LA, Al- Dahmash ND, Ragupathy S, Jayanthi P, Ahn Y-H (2023) Groundnut shell chemically treated with KOH to prepare inexpensive activated carbon: methylene blue adsorption and equilibrium isotherm studies. Environ Res 231:116026. https://doi.org/10.1016/j.envres.2023.116026

McKay G, Al-Duri B (1991) Extended empirical Freundlich isotherm for binary systems: a modified proce dure to obtain the correlative constants. Chem Eng Process 29(3):133–138. https://doi.org/10.1016/0255-2701(91)85012-D

McKay G, Porter JF (1997) Equilibrium parameters for the sorption of copper, cadmium and zinc ions onto peat. J Chem Technol Biotechnol 69(3):309–320. https://doi.org/10.1002/(SICI)1097-4660(199707)69:3%3c309::AID-JCTB724%3e3.0.CO;2-W

Miraboutalebi SM, Nikouzad SK, Peydayesh M, Allahgholi N, Vafajoo L, McKay G (2017) Methylene blue adsorption via maize silk powder: kinetic, equilibrium, thermodynamic studies and residual error analysis. Process Saf Environ Prot 106:191–202. https://doi.org/10.1016/j.psep.2017.01.010

Moradi O, Alizadeh H, Sedaghat S (2022) Removal of pharmaceuticals (diclofenac and amoxicillin) by maltodextrin/reduced graphene and maltodextrin/reduced graphene/copper oxide nanocomposites. Chemosphere 299:134435. https://doi.org/10.1016/j.chemosphere.2022.134435

Murphy OP, Vashishtha M, Palanisamy P, Kumar KV (2023) A review on the adsorption isotherms and design calculations for the optimization of adsorbent mass and contact time. ACS Omega 8(20):17407–17430. https://doi.org/10.1021/acsomega.2c08155

Negarestani M, Farimaniraad H, Mollahosseini A, Kheradmand A, Shayesteh H (2022) Facile preparation of sisal–Fe/Zn layered double hydroxide bio-nanocomposites for the efficient removal of rifampin from aqueous solution: kinetic, equilibrium, and thermodynamic studies. Int J Phytoremed. https://doi.org/10.1080/15226514.2022.2093834

Nodehi R, Shayesteh H, Rahbar-Kelishami A (2022) Fe3O4@NiO core–shell magnetic nanoparticle for highly efficient removal of Alizarin red S anionic dye. Int J Environ Sci Technol 19(4):2899–2912. https://doi.org/10.1007/s13762-021-03399-8

Obar F, Pradhan S, Mackey HR, McKay G (2024) Removal of lithium from aqueous solution by spent coffee ground activated biochar. Process Saf Environ Prot 184:680–689. https://doi.org/10.1016/j.psep.2024.02.020

Pathy A, Krishnamoorthy N, Chang SX, Paramasivan B (2022) Malachite green removal using algal biochar and its composites with kombucha SCOBY: an integrated biosorption and phycoremediation approach. Surf Interfaces 30:101880. https://doi.org/10.1016/j.surfin.2022.101880

Peñafiel ME, Jara-Cobos L, Flores D, Jerves C, Menendez M (2024) Enhancing adsorptive removal of diclofenac from aqueous solution: evaluating organic and inorganic acid treatment of zeolite. Case Stud Chem Environ Eng 9:100575. https://doi.org/10.1016/j.cscee.2023.100575

Poddar K, Sarkar D, Bhoi R, Sarkar A (2024) Biotransformation of diclofenac by isolated super-degrader Pseudomonas sp. DCα4: postulated pathways, and attenuated ecotoxicological effects. Environ Pollut 344:123388. https://doi.org/10.1016/j.envpol.2024.123388

Rajiv P, Mengelizadeh N, McKay G, Balarak D (2021) Photocatalytic degradation of ciprofloxacin with Fe2O3 nanoparticles loaded on graphitic carbon nitride: mineralisation, degradation mechanism and toxicity assessment. Int J Environ Anal Chem. https://doi.org/10.1080/03067319.2021.1890059

Shamsudin MS, Azha SF, Ismail S (2022) A review of diclofenac occurrences, toxicology, and potential adsorption of clay-based materials with surfactant modifier. J Environ Chem Eng 10(3):107541. https://doi.org/10.1016/j.jece.2022.107541

Shayesteh H, Rahbar-Kelishami A, Norouzbeigi R (2016) Evaluation of natural and cationic surfactant modified pumice for congo red removal in batch mode: kinetic, equilibrium, and thermodynamic studies. J Mol Liq 221:1–11. https://doi.org/10.1016/j.molliq.2016.05.053

Shayesteh H, Rahbar-Kelishami A, Norouzbeigi R (2022) Superhydrophobic/superoleophilic micro/nanostructure nickel particles for oil/water mixture and emulsion separation. Ceram Int 48(8):10999–11008. https://doi.org/10.1016/j.ceramint.2021.12.320

Sun M, Sun Q, Zhao C, Huang Y, Jiang J, Ding W, Zheng H (2022) Degradation of diclofenac sodium with low concentration from aqueous milieu through polydopamine-chitosan modified magnetic adsorbent-assisted photo-fenton process. Sep Purif Technol 289:120771. https://doi.org/10.1016/j.seppur.2022.120771

Tawfik AM, Eltabey RM (2024) Fractional kinetic strategy toward the adsorption of organic dyes: finding a way out of the dilemma relating to pseudo-first- and pseudo-second-order rate laws. J Phys Chem A 128(6):1063–1073. https://doi.org/10.1021/acs.jpca.3c07615

Uma Maheswari B, Sivakumar VM, Thirumarimurugan M (2022) Chapter 22 - Synthesis of novel nanobioadsorbent for the effective removal of Pb2+ and Zn2+ ions—Adsorption, equilibrium, modeling, and optimization studies. In: Denizli A, Ali N, Bilal M, Khan A, Nguyen TA (eds) Nano-biosorbents for decontamination of water, air, and soil pollution. Elsevier, pp 503–528. https://doi.org/10.1016/B978-0-323-90912-9.00022-8

Wang J, Zhu H, Hu Y, Hu L, Wei Z, Li YY, Hu X (2025) Mn oxide-modified biochars with high adsorption capacity for Pb(II) in wastewater: preparation and adsorption mechanisms. Environ Res 266:120553. https://doi.org/10.1016/j.envres.2024.120553

Wolska J, Jenczyk J, Zieliński M, Walkowiak-Kulikowska J, Zioła-Frankowska A, Wolski L (2025) Bifunctional adsorbents based on hyper-cross-linked polymers containing carbonyl and amine species for the efficient removal of diclofenac from water in a broad pH range. Environ Res 268:120791. https://doi.org/10.1016/j.envres.2025.120791

Xiao M, Liao Z, Zhou J, Hu J, Li Z (2024) Synthesis of covalent organic framework with amino affinity groups for enhanced selective adsorption of diclofenac sodium from aqueous solution. Sep Purif Technol 346:127467. https://doi.org/10.1016/j.seppur.2024.127467

Yan C, Qu Z, Wang J, Cao L, Han Q (2022) Microalgal bioremediation of heavy metal pollution in water: recent advances, challenges, and prospects. Chemosphere 286:131870. https://doi.org/10.1016/j.chemosphere.2021.131870

Yang C, Huang X, Jin Q, Yang C, Liu D, Li X, Zhou L, Li J, Zhang T, Xia D, Li M, Xie X, Chen H-J (2020) Anomalous dispersion of bioinspired flower-like microparticles for oil/water separation. Nanotechnology 31(9):095712. https://doi.org/10.1088/1361-6528/ab5888

Zuhara S, Pradhan S, McKay G (2023) Investigating mixed biosolids and cardboard for methylene blue adsorption: activation, adsorption modelling and thermodynamics. Environ Res 225:115534. https://doi.org/10.1016/j.envres.2023.115534